CHINESE OPTICS LETTERS

Vol. 21, No. 4 | April 2023

Watt-level laser operation of Pr^{3+}:YLF at 696 and 698 nm

Weihang Cao (曹伟航)[1,2], Zhengdong Dai (戴征东)[1,2], Run Fang (方 润)[1,2,3], Zhongyu Wang (王中玉)[1,2], Yuchen Xue (薛喻宸)[1,2], Bo Xiao (肖 波)[1,2], Huiying Xu (许惠英)[1,2], and Zhiping Cai (蔡志平)[1,2*]

[1] Department of Electronic Engineering, Xiamen University, Xiamen 361005, China

[2] Fujian Key Laboratory of Ultrafast Laser Technology and Applications, Xiamen University, Xiamen 361005, China

[3] School of Physics and Electronic Science, Guizhou Normal University, Guiyang 550001, China

*Corresponding author: zpcai@xmu.edu.cn

Received October 29, 2022 | Accepted December 6, 2022 | Posted Online March 15, 2023

We report continuous-wave deep red lasers at 696.6 and 698.6 nm in a Pr^{3+}:YLF crystal pumped by an InGaN laser diode. A Lyot filter was inserted into the cavity as a birefringent filter to select wavelength; the lasers at 696.6 and 698.6 nm were obtained with a maximum output power of 1.36 and 3.11 W, separately. To the best of our knowledge, the output powers of these two lasers are the highest to date, and this is the first scaling of the output power of the Pr^{3+}:YLF laser to the watt level at around 696 nm. In addition, the corresponding theoretical analysis and simulation were carried out to explain the experimental phenomena.

Keywords: Pr^{3+}:YLF crystal; deep red lasers; Lyot filter.

DOI: 10.3788/COL202321.041404

1. Introduction

Visible solid-state lasers have significantly advanced in power and beam quality, owing to the development of pump sources and crystals[1,2]. The commercially available laser diode (LD)-pumped sources, having the advantages of compactness, high power, and cost-effectiveness, are favored by researchers. Of the many approaches to generate visible lasers, Pr^{3+}-doped materials, one of the successful candidates for high-power efficient solid-state lasers that provide rich laser transitions have aroused much interest in recent years. Various Pr^{3+}-doped materials such as the fluoride crystals[3–10] (Pr^{3+}:$LiYF_4$, Pr^{3+}:$LiGdF_4$, Pr^{3+}:BaY_2F_8, Pr^{3+}:KY_3F_{10}, Pr^{3+}:$LiLuF_4$, etc.), and the oxides crystals[11–15] (Pr^{3+}:$YAlO_3$, Pr^{3+}-Mg^{3+}:$SrAl_{12}O_{19}$, etc.) have been extensively researched. Fluoride crystals have lower crystal field strength and phonon energy compared to oxides, which have greater potential for the development of laser operation. As one of the most common materials for visible lasers, the Pr^{3+}:$LiYF_4$ (YLF) crystal has been shown to feature excellent optics, reasonable mechanical properties, and is a well-known laser gain medium with abundant laser transitions in the visible spectral region[16–21].

In particular, the lasers at 696 and 698 nm in the deep red region have served many different purposes. For instance, the method of obtaining ultraviolet (UV) laser by direct frequency doubling of the deep red laser is more compact and has a higher conversion efficiency than the two-stage nonlinear process to generate a UV laser, which is more suitable for obtaining higher-power UV lasers[22–26]. Additionally, the 696 nm lasers can be used for the spectral analysis of the methanol chlorophyll equation[27], the enzymatic reaction steps of the photoreduction of prochlorophyll-ester[28], and the improvement of the picture resolution of the Cr(III)tris-oxalato complex[29]. The lasers at 698 nm are important not only for research into high-precision atomic clocks[30], but also for nondestructive, real-time, or portable potato quality measurements[31].

To the best of our knowledge, the maximum output power at around 698 nm was reported to be 1.5 W using an optically pumped semiconductor laser (OPSL) as the pump source[32]. However, there are currently few reports of ~696 nm Pr^{3+}:YLF lasers, due to the difficulty of generating lasers with relatively small stimulated emission cross sections. The output power reported at present was relatively lower, with the highest output power of only 116 mW[20,33,34]. Therefore, the deep red lasers based on Pr^{3+}:YLF crystals still have the potential to achieve power scaling.

In this paper, we demonstrate a compact and efficient InGaN LD-pumped Pr^{3+}:YLF crystal to generate deep red lasers at 698.6 nm (π-polarization) and 696.6 nm (σ-polarization). To obtain the lasers in both polarization directions, a Lyot filter was utilized as a birefringent filter to suppress the oscillation of other lasers in the cavity. The maximum output power at 698.6 nm was up to 3.11 W, with a slope efficiency of 31.4%. For the σ-polarization 696.6 nm laser, a maximum output power of 1.36 W was achieved, with a slope efficiency of 15.0%. Notably, both output powers are significantly increased compared to

previous reports, and without saturation. This is the first time to date that the output power of the LD-pumped Pr^{3+}:YLF 696 nm lasers broke into the watt level. Furthermore, theoretical models of the input–output power characteristics were built to explain the results for both wavelengths.

2. Experiment Setup

The schematic setup of the LD-pumped Pr^{3+}:YLF continuous-wave (CW) laser is depicted in Fig. 1. A blue InGaN laser diode with a maximum output power of 24 W was used as the pump source, giving a peak wavelength of approximately 444 nm. As calculated from the relevant parameter manuals, the M^2 factors of the pump source were 46.9 and 15.5 in the x and y directions, respectively. The pump beam was focused into the laser crystal by a plano–convex focusing lens with a focal length of 50 mm. The laser gain medium is a 15-mm-long a-cut Pr^{3+}-doped YLF crystal with 3 mm × 3 mm polished facets (Jiadong Optical Inc., Hefei, Anhui, China). It used the Czochralski method of growth, and the doping concentration is ~0.2% (atomic fraction). A typical plano–concave cavity consisted of an input plane mirror (IM) and an output plano–concave coupler (OC) with a radius of curvature $R = 100$ mm. For the 698 nm laser, the length of the physical cavity was optimized to 98 mm, while at 696 nm, it corresponded to 96 mm.

Figure 2 displays the transmission curves of the IM and OC. The IM has high transmission from 400 to 630 nm and high reflection (> 99.9%) from 690 to 800 nm. The coating of the OC used in the experiment was designed and fabricated in our laboratory using plasma direct-current sputtering technology. To suppress 640 nm laser emission, the IM and OC were coated with high transmissivity of 96.3% and 79.5% at 640 nm, respectively. The OC has a low transmissivity of 2.2% at 696 nm and 2.1% at 698 nm. To protect the crystal as well as laser cavity stability from thermal effect, it was wrapped in indium foil and placed in a copper block, which was kept at 16°C by a water-cooled cooler. The laser crystal was placed close to the IM. The full width at half-maximum (FWHM) of the pump laser spectrum was ~2.2 nm, resulting in a relatively low absorption efficiency of 47% for the crystal.

We inserted a 2-mm thickness Lyot filter with a Brewster angle into the laser resonator to select the wavelength. The operation performance of the single-wavelength 696.6 and 698.6 nm laser was optimized, respectively. To measure the output power,

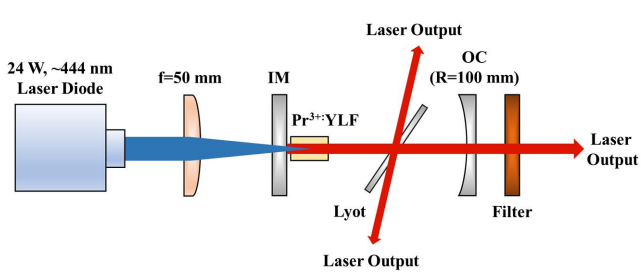

Fig. 1. Schematic experimental setup of the LD-pumped Pr^{3+}:YLF CW laser.

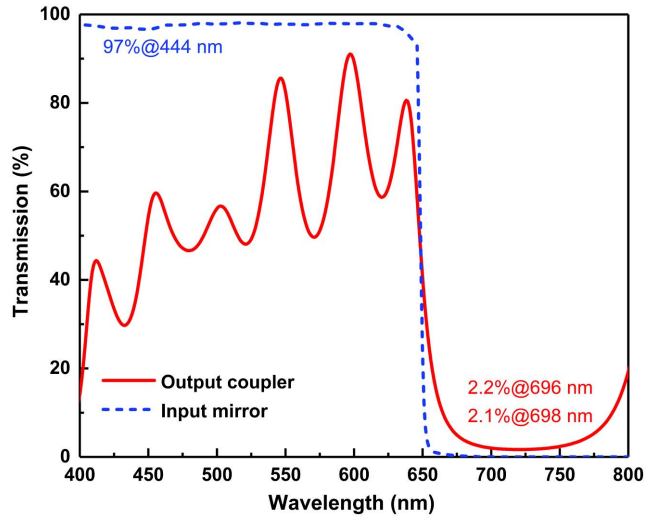

Fig. 2. Transmission curve of IM and OC.

filters with high red transmittance and high blue reflectance were placed behind the output to filter out the pump light. The laser spectra in the experiment were measured by an optical spectral analyzer (Ocean-Optics HR4000+), with a resolution of about 0.25 nm.

3. Result and Discussion

The Pr^{3+}:YLF crystal has various emission lines, for which partial energy level scheme is illustrated in Fig. 3. The 444 nm emission peak of blue InGaN LD matches the ground state absorption of $^3H_4 \rightarrow {}^3P_2$. The lasers at 696.6 and 698.6 nm were based on a four-level system operation. The population is excited from the ground-state energy level ($^3H_4$) to the $^3P_2$ level by the pump source, and then rapidly relaxes to the metastable $^3P_0$ level (denoted by Γ_1). The $^3F_3$ energy level is split into several Stark sublevels due to crystal field effect[35]. Following the electric-dipole selection rules, the lasers at 696.6 nm (σ-polarization, $\Gamma_1 \rightarrow \Gamma_{3,4}$) and 698.6 nm (π-polarization, $\Gamma_1 \rightarrow \Gamma_2$) are

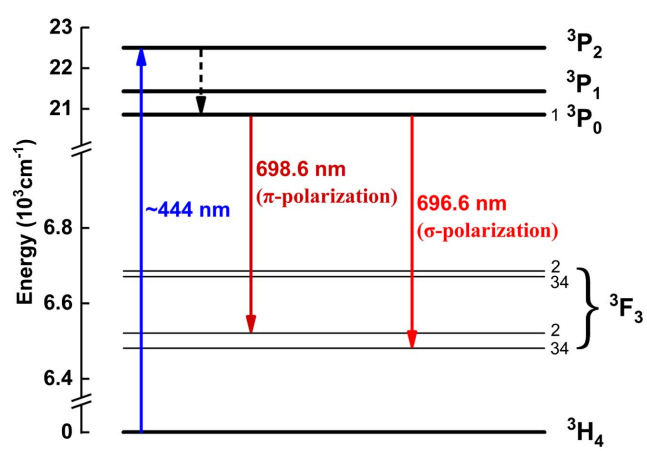

Fig. 3. Partial energy level scheme of Pr^{3+}:YLF crystal.

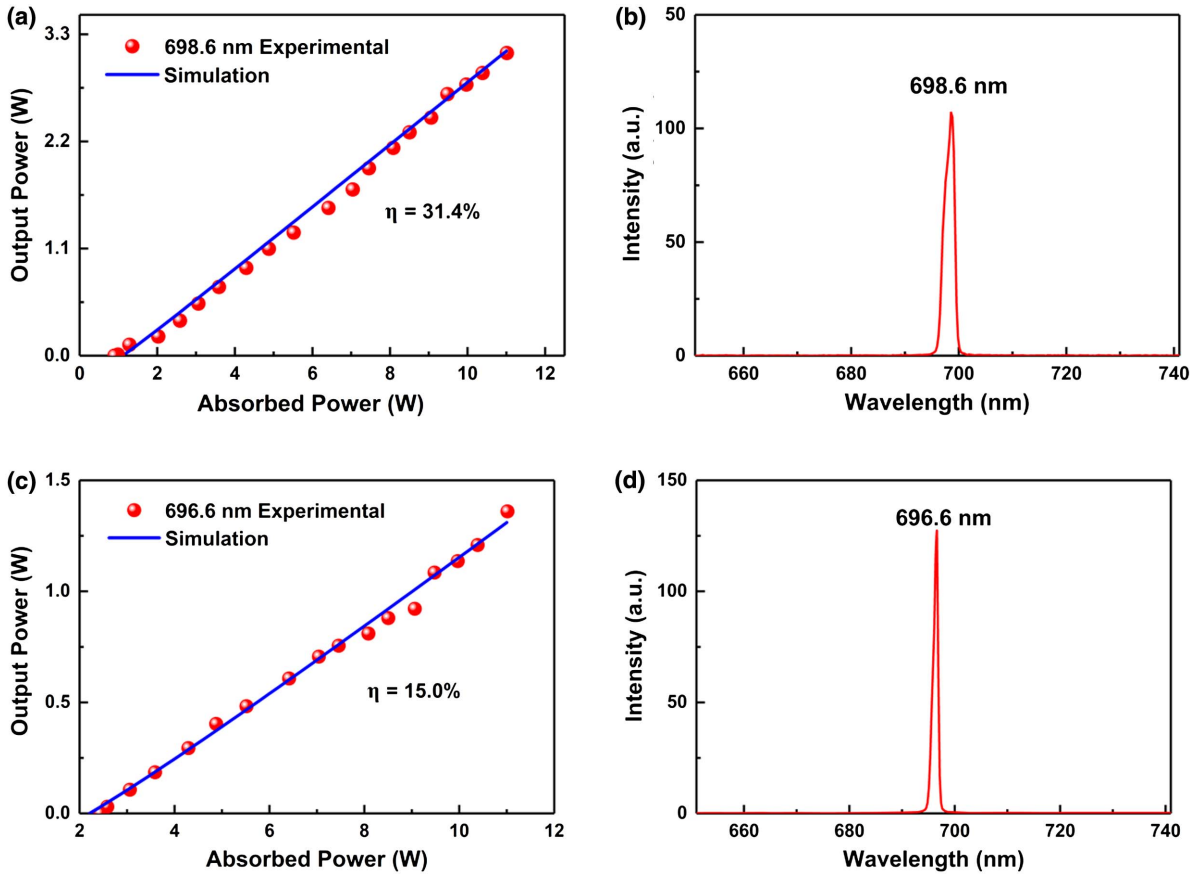

Fig. 4. Laser output performance at 698.6 and 696.6 nm. (a), (c) Experimental input–output relationship and simulation results; (b), (d) laser emission spectra of 698.6 and 696.6 nm.

generated by the transition from the $^3P_0$ level to the $^3F_3$ different sublevels.

Figure 4 depicts the laser output characteristics. The spectra were measured at the maximum output power with emission peaks at 698.6 and 696.6 nm, respectively [see Figs. 4(b)–4(d)]. According to the previous studies on spectral analysis,[4] the emission cross sections at 696 and 698 nm are smaller relative to 721 nm ($^3P_0 \rightarrow {}^3F_4$). In addition, the positions at 696 and 698 nm are relatively close to the position at 721 nm in the spectrum. Thus, it is difficult to suppress the laser transition at 721 nm with the mirror manufactured in our laboratory. The Lyot filter with a Brewster angle was inserted into the cavity and rotated by a certain angle to obtain the π-polarized 698.6 nm laser [see Fig. 4(a)]. The maximum output power was 3.11 W with a threshold power of 0.9 W; the slope efficiency was 31.4%. The M^2 factors were measured to be 3.1 and 2.3 in the x and y directions, respectively [Fig. 5(b)]. Similarly, by tuning the Lyot filter to the optimal position, we achieved the 696.6 nm laser in the σ-polarization direction with a maximum output power of 1.36 W, a slope efficiency of approximately 15.0%, and a threshold power of 2.44 W, as shown in Fig. 4(c). The beam M^2 was 1.8 and 2.2 in the x and y directions, respectively [Fig. 5(a)]. The embedded output beam images were captured by a CCD. It is worth emphasizing that due to the insertion of the Lyot filter in the resonant cavity, we measured the laser power as a triple-end output. The tail-end output power is 1.23 W (696.6 nm) and 1.33 W (698.6 nm) under the maximum input power, respectively. As can be seen in Figs. 5(c) and 5(d), the stability of the output power was recorded every 5 min for a monitoring time of 1 h. The corresponding power fluctuations at 696.6 and 698.6 nm were 0.46% and 0.52%, respectively. In addition, the maximum output powers are the highest known and have good linearity with no saturation.

To better understand the experimental results, we performed some theoretical simulations on the relationship between output power and absorbed pump power. For a four-level laser system, the input–output characteristics can be determined by[36]

$$P_{\text{in}} = \frac{A_e \gamma I_{\text{sat}}}{\eta_p}\left[\int_a \frac{\in(x,y,z)g(x,y,z)}{(2P_{\text{out}}/TA_eI_{\text{sat}})\in(x,y,z)+1}\,\mathrm{d}V\right]^{-1}, \quad (1)$$

where η_p indicates the pumping efficiency, γ indicates the logarithmic loss per pass, A_e indicates the effective mode area of the lasing mode, and I_{sat} indicates the saturation intensity. The power transmission in the laser is denoted with T, and the normalized pump distribution inside the active material is denoted with g. P_{in} and P_{out} are the input and output power, respectively. The equation for the dimensional mode distribution factor of the laser beam (∈) is

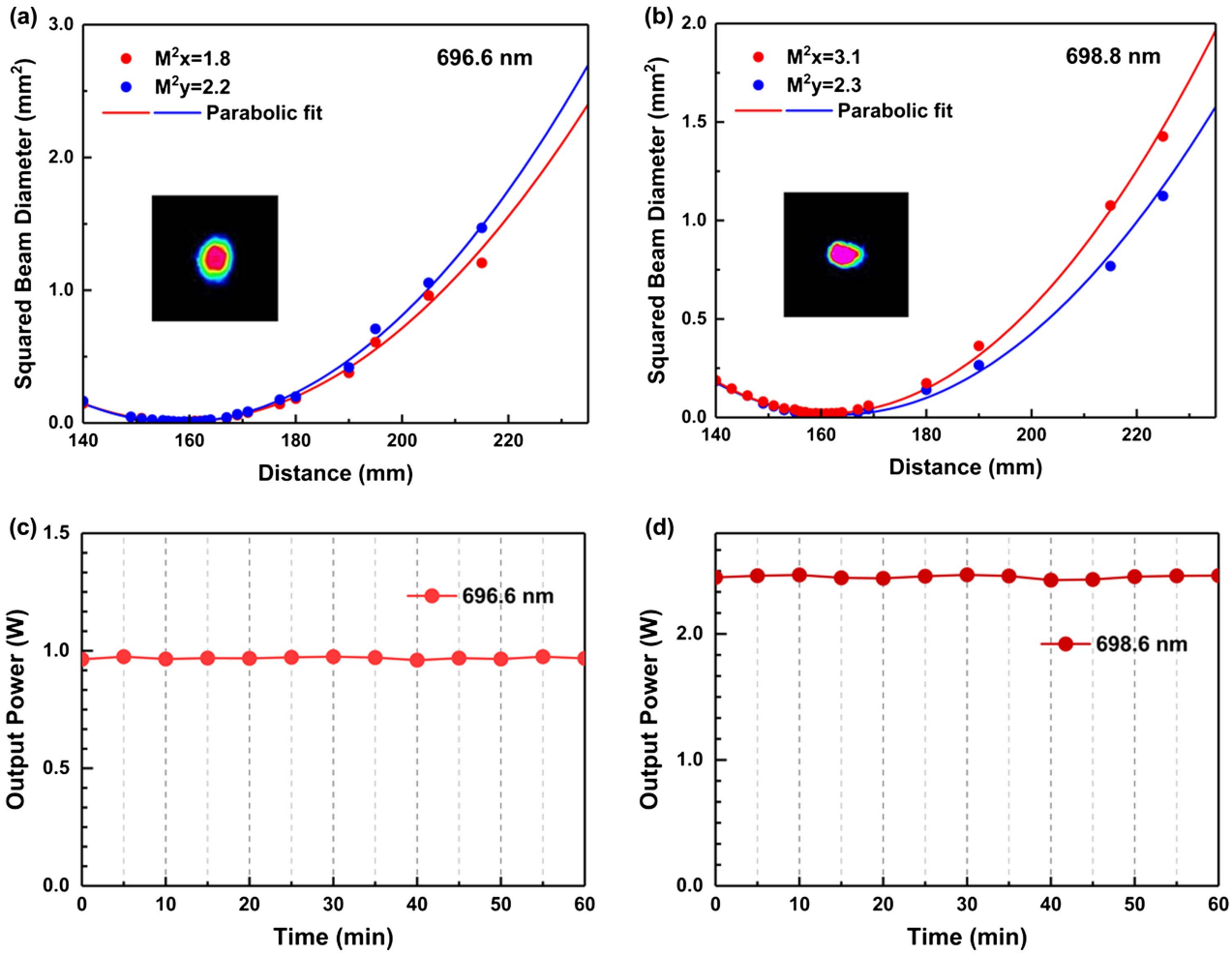

Fig. 5. (a), (b) Measured corresponding M^2 factors of 696.6 and 698.6 nm, respectively; (c), (d) power stabilities of lasers at 696.6 and 698.6 nm.

$$e^{\frac{-2(x^2+y^2)}{\omega^2}}, \tag{2}$$

where ω represents the laser waist radius. When considering P_{out} is limited to zero, we can write the equation as

$$P_{\text{th}} = \frac{A_e \gamma I_{\text{sat}}}{\eta_p \int_a \in g \mathrm{d}V}, \tag{3}$$

where P_{th} is the threshold power, and the integral $\int_a \in g\mathrm{d}V$ considers the spatial overlapping of pump and mode distribution.

For a circular Gaussian laser beam, by introducing the parameter $\alpha = (\omega/\varpi_p)^2$, some analytical solution can be obtained,

$$P_{\text{out}} = \frac{T}{2\gamma}\eta_p \frac{\alpha(\alpha+2)}{(1+\alpha)^2}[P_{\text{in}} - P_{\text{th}}(\alpha)], \tag{4}$$

$$P_{\text{th}} = \frac{\pi\gamma I_{\text{sat}}\varpi_p^2}{2\eta_p}(1+\alpha), \tag{5}$$

where ϖ_p is the average pump light waist radius ($\omega = \varpi_p$). Through Eqs. (4) and (5), the output powers and thresholds of the Pr^{3+}:YLF lasers can be estimated and calculated based on the emission cross sections and lifetime as well as the laser geometer. The parameters we used in the simulations are listed in Table 1.

As can be seen from Table 1, the laser emission cross section at 698 nm is 9.79×10^{-20} cm^2, which is much larger than 1.51×10^{-20} cm^2 at 696 nm. But the threshold power of the two wavelengths only differs by a factor of over 2. This is owing to the saturation intensity of the 696 nm which is 7 times more than that of 698 nm. The 696.6 nm laser with smaller emission cross section requires a decrease in the average pump light waist radius to reduce the threshold power of the laser, and reducing the average pump size is beneficial in improving the output

Table 1. Parameters Used in the Simulation of Lasers at 698 and 696 nm.

λ (nm)	σ_e (10^{-20} cm^2)	I_{sat} (mW/μm^2)	ϖ_p (μm)	γ	T (%)
696	1.51	5.106	75	0.0155	0.42
698	9.79	0.785	108	0.023	1.55

power. The difference in loss (γ) between the two wavelengths is mainly attributed to the different angles of the adjusted Lyot filter. Thus, the high emission cross section and low cavity loss are key parameters to achieve high power and high slope efficiency.

4. Conclusion

In summary, we reported LD-pumped Pr^{3+}:YLF CW deep red lasers. By inserting a Lyot filter and optimizing the laser resonant cavity, the π-polarized 698.6 nm laser and σ-polarized 696.6 nm laser were obtained, respectively. For π-polarization, the maximum output power was up to 3.11 W. The slope efficiency was 31.4%, and no output saturation power was observed. A similar trend also existed for the σ-polarization: a maximum output power of 1.36 W was measured with a slope efficiency of 15.0%. To the best of our knowledge, the output power of these two wavelengths is by far the highest for an LD-pumped Pr^{3+}:YLF crystal. This represents the first time to date that the output power of an LD-pumped Pr^{3+}:YLF laser at 696 nm reached the watt level, which is 10 times higher than the previously reported. Moreover, theoretical simulations were performed to explain the relationship between the output laser power and the absorbed pump power, which were consistent with the experimental results. With the continuous development of solid-state deep red lasers, it is expected to expand the application prospects in the visible region and achieve high-power UV lasers by frequency doubling.

Acknowledgement

This work was supported by the National Natural Science Foundation of China (No. 61975168).

References

1. C. Kränkel, D. T. Marzahl, F. Moglia, G. Huber, and P. W. Metz, "Out of the blue: semiconductor laser pumped visible rare-earth doped lasers," Laser Photonics Rev. **10**, 548 (2016).
2. H. Tanaka, S. Kalusniak, M. Badtke, M. Demesh, N. V. Kuleshov, F. Kannari, and C. Kränkel, "Visible solid-state lasers based on Pr^{3+} and Tb^{3+}," Prog. Quantum. Electron. **84**, 100411 (2022).
3. A. Richter, E. Heumann, E. Osiac, G. Huber, W. Seelert, and A. Diening, "Diode pumping of a continuous-wave Pr^{3+}-doped $LiYF_4$ laser," Opt. Lett. **29**, 2638 (2004).
4. T. Gün, P. Metz, and G. Huber, "Power scaling of laser diode pumped Pr^{3+}:$LiYF_4$ cw lasers: efficient laser operation at 522.6 nm, 545.9 nm, 607.2 nm, and 639.5 nm," Opt. Lett. **36**, 1002 (2011).
5. Y. Y. Ren, Z. M. Cui, L. F. Sun, C. Wang, H. L. Liu, and Y. J. Cai, "Laser emission from low-loss cladding waveguides in Pr:YLF by femtosecond laser helical inscription," Chin. Opt. Lett. **20**, 122201 (2022).
6. F. Cornacchia, A. Di Lieto, M. Tonelli, A. Richter, E. Heumann, and G. Huber, "Efficient visible laser emission of GaN laser diode pumped Pr-doped fluoride scheelite crystals," Opt. Express **16**, 15932 (2008).
7. D. Pabœuf, O. Mhibik, F. Bretenaker, P. Goldner, D. Parisi, and M. Tonelli, "Diode-pumped Pr:BaY_2F_8 continuous-wave orange laser," Opt. Lett. **36**, 280 (2011).
8. P. Camy, J. L. Doualan, R. Moncorgé, J. Bengoechea, and U. Weichmann, "Diode-pumped Pr^{3+}:KY_3F_{10} red laser," Opt. Lett. **32**, 1462 (2007).
9. A. S. Rao, T. Miike, K. Miyamoto, and T. Omatsu, "Optical vortex lattice mode generation from a diode-pumped Pr^{3+}:$LiYF_4$ laser," J. Opt. **23**, 075502 (2021).
10. A. Sottile, Z. Zhang, S. Veronesi, D. Parisi, A. D. Lieto, and M. Tonelli, "Visible laser operation in a Pr^{3+}:$LiLuF_4$ monocrystalline fiber grown by the micro-pulling-down method," Opt. Mater. Express **6**, 1964 (2016).
11. M. Fibrich and H. Jelínková, "Power-scaled Pr:$YAlO_3$ laser at 747 and 720 nm wavelengths," Laser Phys. Lett. **10**, 035801 (2013).
12. M. Fechner, F. Reichert, N.-O. Hansen, K. Petermann, and G. Huber, "Crystal growth, spectroscopy, and diode pumped laser performance of Pr,Mg:$SrAl_{12}O_{19}$," Appl. Phys. B **102**, 731 (2011).
13. M. Fibrich, J. Šulc, and H. Jelínková, "Pr:$YAlO_3$ laser performance enhancement by operating the laser close to liquid helium temperatures," Opt. Laser Technol. **148**, 107653 (2022).
14. H. Chen, H. Uehara, H. Kawase, and R. Yasuhara, "Efficient Pr:$YAlO_3$ lasers at 622 nm, 662 nm, and 747 nm pumped by semiconductor laser at 488 nm," Opt. Express **28**, 3017 (2020).
15. L. B. Zhou, J. Y. Zou, W. X. Zheng, T. Zhang, B. Xu, X. D. Xu, A. A. Lyapin, and J. Xu, "More than 2.3 W diode-pumped quasi-continuous-wave Pr, Mg:$SrAl_{12}O_{19}$ bulk laser and the first demonstration of Co:ZnSe-based passively *Q*-switched deep red laser at 724 nm," Opt. Laser Technol. **145**, 107471 (2022).
16. B. Xu, Z. Liu, H. Xu, Z. P. Cai, C. Zeng, S. Huang, Y. Yan, F. Wang, P. Camy, J. L. Doualan, A. Braud, and R. Moncorge, "Highly efficient InGaN-LD-pumped bulk Pr:YLF orange laser at 607 nm," Opt. Commun. **305**, 332 (2013).
17. Y. J. Cheng, B. Xu, B. Qu, S. Y. Luo, H. Yang, H. Y. Xu, and Z. P. Cai, "Comparative study on diode-pumped continuous wave laser at 607 nm using differently doped Pr^{3+}:$LiYF_4$ crystals and wavelength tuning to 604 nm," Appl. Opt. **53**, 7898 (2017).
18. B. Xu, P. Camy, J. L. Doualan, Z. P. Cai, and R. Moncorge, "Visible laser operation of Pr^{3+}-doped fluoride crystals pumped by a 469 nm blue laser," Opt. Express **19**, 1191 (2011).
19. B. Qu and Q. Huang, "Watt-level diode-pumped continuous-wave Pr:$LiYF_4$ laser at 670 nm and simultaneous dual-wavelength operation at 639 and 670 nm," Appl. Opt. **59**, 3033 (2020).
20. Z. Liu, Z. P. Cai, B. Xu, S. L. Huang, C. H. Zeng, Y. Yan, F. J. Wang, H. Y. Xu, J. L. Doualan, P. Camy, and R. Moncorgé, "Continuous-wave laser emission of Pr:$LiYF_4$ at 695.8 nm," IEEE Photon. Technol. Lett. **26**, 675 (2014).
21. Z. Liu, Z. P. Cai, S. L. Huang, C. H. Zeng, Z. Y. Meng, Y. K. Bu, Z. Q. Luo, B. Xu, H. Y. Xu, C. C. Ye, F. Stareki, P. Camy, and R. Moncorgé, "Diode-pumped Pr^{3+}:$LiYF_4$ continuous-wave deep red laser at 698 nm," J. Opt. Soc. Am. B **30**, 302 (2013).
22. V. Ostroumov, W. Seelert, L. Hunziker, C. Ihli, A. Richter, E. Heumann, and G. Huber, "UV generation by intracavity frequency doubling of an OPS-pumped Pr:YLF laser with 500 mW of cw power at 360 nm," Proc. SPIE **6451**, 645103 (2007).
23. N. Niu, S. Pu, Q. Chen, Q. Chen, Y. Wang, Y. Zhao, W. Wu, and Q. Zheng, "302 nm continuous wave generation by intracavity frequency doubling of a diode-pumped Pr:YLF laser," Appl. Opt. **57**, 9798 (2018).
24. Z. Liu, Z. P. Cai, B. Xu, C. H. Zeng, S. L. Huang, F. J. Wang, Y. Yan, and H. Y. Xu, "Continuous-wave ultraviolet generation at 349 nm by intracavity frequency doubling of a diode-pumped Pr:$LiYF_4$ laser," IEEE Photon. J. **5**, 1500905 (2013).
25. A. Srinivasa Rao, N. Apurv Chaitanya, and G. K. Samanta, "High-power, high repetition-rate, ultrafast fibre laser based source of DUV radiation at 266 nm," OSA Contin. **2**, 99 (2019).
26. Y. S. Zhang, J. Y. Zou, W. X. Zheng, K. Feng, B. Xu, and Z. F. Yu, "Watt-level continuous-wave intracavity frequency-doubled Pr:YLF-LBO laser at 320 nm," Chin. Opt. Lett. **19**, 091406 (2021).
27. R. J. Ritchie, "Consistent sets of spectrophotometric chlorophyll equations for acetone, methanol and ethanol solvents," Photosyn. Res. **89**, 27 (2006).
28. D. J. Heyes and C. N. Hunter, "Making light work of enzyme catalysis: protochlorophyllide oxidoreductase," Trends Biochem. Sci. **30**, 642 (2005).
29. G. L. J. A. Rikken and E. Raupach, "Enantioselective magnetochiral photochemistry," Nature **405**, 932 (2000).
30. M. G. Tarallo, N. Poli, M. Schioppo, D. Sutyrin, and G. M. Tino, "A high-stability semiconductor laser system for a 88 Sr-based optical lattice clock," Appl. Phys. B **103**, 17 (2011).

31. Z. Zhou, S. W. Zeng, X. Y. Li, and J. Zheng, "Nondestructive detection of blackheart in potato by visible/near infrared transmittance spectroscopy," J. Spectrosc. **2015**, 786709 (2015).
32. P. W. Metz, F. Reichert, F. Moglia, S. Müller, D. T. Marzahl, C. Kränkel, and G. Huber, "High-power red, orange, and green Pr^{3+}:$LiYF_4$ lasers," Opt. Lett. **39**, 3193 (2014).
33. B. Xu, Y. J. Cheng, B. Qu, S. Y. Luo, H. Y. Xu, Z. P. Cai, P. Camy, J. L. Doualan, and R. Moncorgé, "InGaN-LD-pumped Pr^{3+}:$LiYF_4$ continuous-wave deep red lasers at 697.6 and 695.8 nm," Adv. Opt. Photonics **67**, 146 (2015).
34. S. Y. Luo, B. Xu, S. W. Cui, H. Chen, Z. P. Cai, and H. Y. Xu, "Diode-pumped continuous-wave dual-wavelength c-cut Pr^{3+}:$LiYF_4$ laser at 696 and 719 nm," Appl. Opt. **54**, 10051 (2015).
35. L. Esterowitz, F. J. Bartoli, R. E. Allen, D. E. Wortman, C. A. Morrison, and R. P. Leavitt, "Energy levels and line intensities of Pr^{3+} in $LiYF_4$," Phys. Rev. B **19**, 6442 (1979).
36. P. Laporta and M. Brussard, "Design criteria for mode size optimization in diode-pumped solid-state lasers," IEEE J. Quantum Electron. **27**, 2319 (1991).